Wu et al. *EPJ Quantum Technology* (2023) 10:12
https://doi.org/10.1140/epjqt/s40507-023-00169-y

EPJ Quantum Technology
a SpringerOpen Journal

EPJ.org

RESEARCH Open Access

Quantum-enhanced receiver for quadrature phase shift keying using conjugated homodyne detection

Tianyi Wu[1], Yang Ran[1], Zichao Zhou[1], Chang Guo[1], Kai Li[1] and Chen Dong[1*]

*Correspondence:
dongchengfkd@163.com
[1]Information and Communication College, National University of Defense Technology, Wuhan, China

Abstract

Coherent detection (homodyne detection/heterodyne detection) and single photon detection are commonly applied in classical communication and quantum communication/receiver respectively. In this paper, we firstly propose a quantum-enhanced receiver based on conjugated homodyne detection, which is consisted of two classical balanced homodyne detectors, for discrimination among quadrature-phase-modulated weak coherent states. Our detection part works as a photon counter in every single-shot measurement during the process of detection and feedback, which could help our quantum-enhanced receiver surpass the standard quantum limit when an optimized detection threshold τ from 0.05 to 0.3 is selected. Moreover, our proposed quantum-enhanced receiver with conjugated homodyne detectors can obtain the same low error probability as conventional quantum-enhanced receivers (with its superconducting nanowire single photon detectors' detection efficiency 60% for pulse separation $M = 8$ and 70% for $M = 12$ under the same adaptive feedback countermeasures.) Meanwhile, our scheme of the quantum-enhanced receiver gains its incomparable advantages on room-temperature working condition and low cost due to the application of conjugated homodyne detectors. As far as we concerned, this is the first time to explore the performance of the quantum-enhanced receiver with commercial homodyne detectors. And the analysis in this paper may pave the way to reduce the cost of the quantum-enhanced receiver and make it more adaptable for long-distance optical communication systems.

Keywords: Quantum-enhanced receiver; Conjugated homodyne detector; QPSK coherent states discrimination

1 Introduction

Precise discrimination of non-orthogonal coherent states remains an everlasting puzzle for decades due to the intrinsic overlap among those states [1]. Efficient measurements and discrimination strategies for these non-orthogonal states have been proposed and applied to many related fields, such as quantum computation [2, 3], quantum-enhanced metrology [4–6] and quantum key distribution (QKD) [7–9]. However, when conventional receivers with homodyne or heterodyne measurement were applied to discriminate those

Springer

non-orthogonal states from weak signals, their detection performance of discrimination error obtainable would be limited to be below shot-noise limit [1] due to intrinsic noises. And the error probability given by conventional detection measurements was defined as the standard quantum limit (SQL). Moreover, when comes to deal with weak signals with lower signal-noise-ratio, a quantum-enhanced receiver was put forward to surpass the SQL even to approach the ultimate minimum discrimination error limit—"Helstrom bound" (HB) by quantum mechanics [1].

The proposed quantum-enhanced receiver generally consists of a displacement operator, an optical coupler and a single photon detector (SPD). Once the signal with encoded coherent states is displaced to a photon number state by interference through the effort of the displacement operator in an optical coupler, the SPD will "click" as the response for the detection event "photons received", and null detection for no photons. Therefore, the precise detection towards photon number state—"click or not" of SPD will affect the performance of the quantum-enhanced receiver. The application of superconducting transition-edge sensors (TES) which enabled the single-photon-level detection, could be the start of experimental demonstration of the quantum-enhanced receiver in 2011 [10]. Later on, sorts of SPDs with higher efficiency and less dark count rate, like superconducting single photon detectors (SSPD) or superconducting nanowire single photon detectors (SNSPD), were widely applied to the quantum-enhanced receiver [11–15]. To further reduce the error rate of photon detection, as summarized in [16], photon number resolving detector (PNRD), which could distinguish the number rather than only the existence of the photons, was applied to the quantum-enhanced receiver [17–20]. And their below-SQL performance was dramatically extended to higher input energies (larger photon numbers).

Though the sorts of SPDs (including TES) have made the experimental demonstration of the quantum-enhanced receiver come true, their high cost, large size and tough experimental condition (ultra-low working temperature under near-perfect vacuum) have also slowed down the pace of putting the lab-based quantum-enhanced receiver into practice. Coincidentally, noted that conjugated homodyne detectors, which is more affordable and able to work at room temperature, have been tested to measure conjugated quadrature and reconstruct photon number statistics of the input weak states [21]. Soon, the advantage on cost-effective and high-bandwidth of conjugated homodyne detectors has been further exploited, they have been applied to polarization encoding [22, 23] and phase encoding [24] discrete variable QKD. Inspired by the application of conjugated homodyne detectors on discriminating the input states in BB84 QKD under "photon counting" mode [22], we come up with an idea that the conjugated homodyne detectors are worth testing in the quantum-enhanced receiver to recover detected photon number so as to discriminate the input coherent states.

In this paper, we explore the performance of the conjugated homodyne detectors operated in our scheme of quantum-enhanced receiver for the first time. Relative theoretical analysis and simulations are made to discriminate the quadrature phase shift keying (QPSK) coherent states. It is worthy noted that through the proper selection on the detection threshold, we achieve a balance between the detection efficiency and the dark count rate of the detectors. And the conjugated homodyne detection quantum-enhanced receiver, which we called CHD quantum-enhanced receiver, could even match the performance of the quantum-enhanced receiver with high-detection-efficiency SNSPDs.

The paper is organized as follows: In Sect. 2, we first introduce the basic theory of quantum-enhanced receiver for QPSK coherent states. In Sect. 3, we demonstrate QPSK coherent states discrimination via our proposed CHD quantum-enhanced receiver. In Sect. 4, we discuss our simulation results of the proposed CHD quantum-enhanced receiver, while the conclusion is summarized in Sect. 5.

2 Quantum-enhanced receiver with feedback for discriminating QPSK coherent states

In this section, we introduce a conventional quantum-enhanced receiver with feedback for the discrimination of the QPSK coherent states.

The input QPSK coherent states can be defined as $|\alpha_k\rangle = ||\alpha|e^{\frac{(2k+1)i\pi}{4}}\rangle$, where $k = 0, 1, 2, 3$ and $|\alpha|$ represents the amplitude of the input signal state.

Figure 1 depicts a scheme of a conventional quantum-enhanced receiver with feedback operation. The quantum-enhanced receiver consists of a displacement preparation part, a beam splitter, a single-photon detector and a corresponding real-time feedback control on displacement operation based on detection history of the SPD.

In our scheme, the process of the whole quantum-enhanced receiver could be concluded as: An input QPSK coherent signal state with one spatial mode, prepared in a square pulse with a time width of T, would be virtually separated to M parts. During ith part of the whole signal pulse ($i = 1, 2, \ldots, M$), a displacement operator $\hat{D}(\beta_i)$, firstly prepared under random choice from the QPSK states, will be combined together with the signal state in a beam splitter to shift the ith signal coherent state into photon number state via interference. Once the displacement operator $\hat{D}(\beta_i)$ is prepared as same as the signal state, the shifted state will be a vacuum state, otherwise photons will be left. Correspondingly, the SPD will provide a binary detection outcome $e_i \in \{0, 1\}$ or represented as Eq. (1) in positive-operator-valued measures (POVMs) method [25].

$$\begin{cases} \hat{\Pi}_0 = e^{-\nu} \sum_{n=0}^{\infty} (1-\eta)^n |n\rangle\langle n|, \\ \hat{\Pi}_1 = \hat{I} - \hat{\Pi}_0, \end{cases} \tag{1}$$

where ν is denoted as the dark count rate and η represents the detection efficiency of the SPD. Thus the probability of detection outcome could be given by Ref. [14]:

$$\begin{aligned} P(e_i|\alpha_k;\beta_i) &= \langle\alpha_k|\hat{D}\dagger(-\beta_i)\hat{\Pi}_{e_i}\hat{D}\dagger(-\beta_i)|\alpha_k\rangle \\ &= (1-e_i)e^{-\nu-\eta|\alpha_k-\beta_i|^2} + e_i\left(1-e^{-\nu-\eta|\alpha_k-\beta_i|^2}\right). \end{aligned} \tag{2}$$

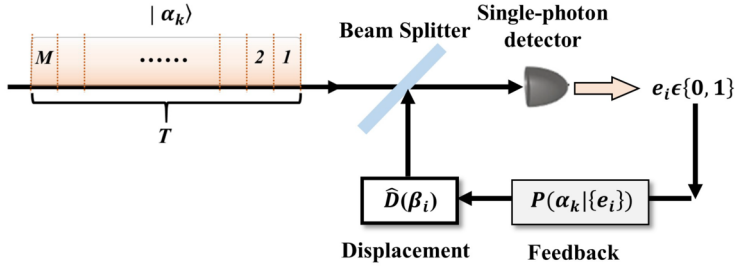

Figure 1 A quantum-enhanced receiver with a beam splitter, displacement, single photon detection and feedback operations for discrimination of QPSK coherent states

And once the displacement operator $\hat{D}(\beta_i)$ has the same amplitude as the amplitude $|\gamma|$ of the signal state $|\alpha_k\rangle$, the photon number $|\alpha_k - \beta_i|^2$ of the interference light in Eq. (2) can be described as:

$$|\alpha_k - \beta_i|^2 = 2(1 - \xi \cos\theta)|\gamma|^2, \tag{3}$$

where θ is the relative phase between the displacement operator $\hat{D}(\beta_i)$ and the signal state $|\alpha_k\rangle$ from QPSK protocol. ξ is the interference visibility which can characterize the mismatch between input signal and displacement operator (such mismatch can be originated from differences on amplitude, polarization, frequency, spatial and temporal modes as well as phase noise [19]).

The detection outcomes of the SPD will be recorded in a history outcome group $\{\beta_i, e_i\}$ which will be regarded as a priori belief. Corresponding feedback control towards the displacement preparation part will refer to the history outcome group: Once the detection outcome is off ($e_i = 0$), which means that a destructive interference occurred between the same QPSK coherent states of the signal and the displacement operator, the current belief will be enhanced, and the current displacement operator will be maintained for the next step in the $(i+1)$th part; As the detection outcome is on ($e_i = 1$), which strongly indicates that the signal state was not shifted to vacuum state by the displacement operator. Hence, the current displacement operator will be changed to another state in the QPSK coherent states. Based on Bayesian theorem, the feedback operator could be obtained by a posteriori probability $P(\alpha_k|\{\beta_i, e_i\})$ after detection of the ith part [26]. A more detailed process of feedback will be illustrated in Appendix A.

Similar to the Ref. [14], based on the schematic of the conventional quantum-enhanced receiver with feedback in Fig. 1, together with Eq. (2) and Eq. (A) in Appendix A, the average error probability for distinguishing the QPSK coherent states could be obtained as:

$$P_e = 1 - \frac{1}{4}\sum_{k=0}^{3}\sum_{\{\beta_i,e_i\}\in\Theta_k} P\big(\{\beta_i, e_i\}|\alpha_k\big), \tag{4}$$

where the conditional probability $P(\{\beta_i, e_i\}|\alpha_k)$ represents the probability of having the historical detection outcome $\{\beta_i, e_i\}$ when the input coherent state $|\alpha_k\rangle$ is prepared. And Θ_k is denoted as the group of detection outcome when the input state $|\alpha_k\rangle$ is received. Therefore, a model could be constructed by the evaluation on the error probability with imperfections through the Eq. (4).

The ideal SQL bound for discriminating QPSK coherent states [14] could be calculated by:

$$P_e(\mathrm{SQL}) = 1 - \frac{1}{4}\left[1 + \mathrm{erf}\left(\frac{|\alpha|}{\sqrt{2}}\right)\right]^2, \tag{5}$$

where $\mathrm{erf}\, x$ is the error function.

Another ultimate limit—Helstrom bound, could also be well approximate calculated by using the square-root measurement according to Ref. [1, 27].

$$P_e(\mathrm{HB}) = 1 - \frac{1}{16}\left[\sum_{i=1}^{4}\sqrt{e^{-|\alpha|^2}\sum_{k=1}^{4} e^{(1-i)\frac{ik\pi}{2} + |\alpha|^2 e^{\frac{ik\pi}{2}}}}\right]^2. \tag{6}$$

3 Quantum-enhanced receiver using conjugated homodyne detection for discriminating QPSK coherent states

The exploration of the conjugated homodyne detection scheme in [21] convinces its ability of discriminating photon number states and recovering photon statistics in both single-shot measurement and repeated measurement, respectively. When operated in single-shot measurement, the conjugated homodyne detectors could inherit the function of photon counting from the conventional threshold SPD, which has been tested in the application on polarization-encoded BB84 QKD [22, 23].

In this section, we introduce our quantum-enhanced receiver based on the conjugated homodyne detection scheme for the discrimination of input QPSK coherent quantum states in every single-shot measurement. And our proposed structure of the CHD quantum-enhanced receiver is shown in Fig. 2.

Our proposed quantum-enhanced receiver could be divided as two main parts: states preparation region (Region I) and conjugated homodyne detection region (Region II). The proposed receiver is operated as follows: In Region I, telecom-band laser pulses light from a CW laser #1 is modulated as pulses by an intensity modulator and divided into two parts: a weak part and a strong part. They are prepared as input coherent states $|\alpha_k\rangle$ and displacement operators $\hat{D}(\beta_i)$, respectively. Both $|\alpha_k\rangle$ and $\hat{D}(\beta_i)$ are random-phase modulated from QPSK protocol. Then the displacement operator shift the signal coherent state into photon number state (Fock state $|n\rangle$) via interference as they are both coupled into a 2×1 unsymmetric optical coupler. The output interferenced beam from the coupler is supposed to be detected by single photon detectors in a conventional quantum-enhanced receiver. And the basic theory of a conventional quantum-enhanced receiver for discriminating QPSK coherent states in Region I has been illustrated in Sect. 2 and the simulation model of the parts from states preparation to displacement operation (interference) could be built from Eqs. (1)–(4).

While in our proposed CHD quantum-enhanced receiver, in the detection part (Region II), conjugated homodyne detector takes the place of the conventional single photon detectors to explore whether the photon number states after interference is vaccum or not. In Region II, the output interferenced beam is regarded as the weak signal (S) of the conjugated homodyne detector and modulated pulses from a CW laser #2 (we assume both laser #1 and laser #2 have the same spatial mode, polarization and frequency) are re-

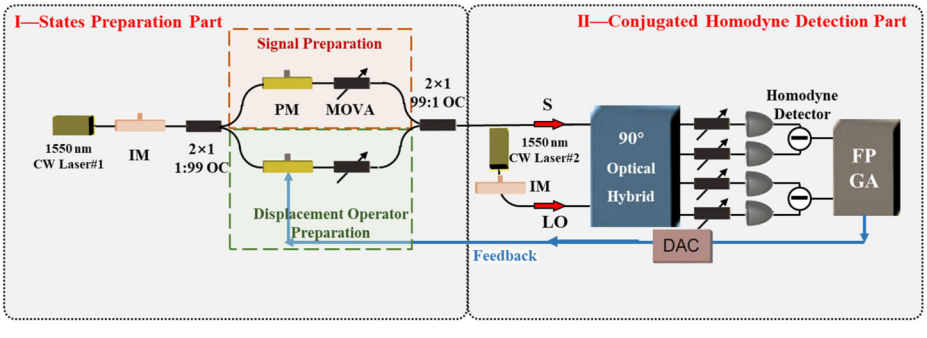

Figure 2 The schematic of a CHD quantum-enhanced receiver for discriminating QPSK coherent states. CW, continuous-wave; IM, intensity modulator; OC, optical coupler; PM, phase modulator; MOVA, manual optical variable attenuator; S, signal; LO, local oscillator; FPGA, field programmable gate array; DAC, digital-to-analog converter

garded as local oscillator (LO). Then both the LO and the S are coupled into the following conjugated homodyne detector. Consisting of a 90° optical hybrid and two homodyne detectors (here we assume 4 noiseless detectors with unity efficiency η_{det}), the conjugated homodyne detectors can simultaneously measure a pair of the detected outputs (quadrature components X and P) in every single-shot measurement. And the observable probability parameter of detection output Z, has been defined to describe these two components in theory [21]:

$$Z = X^2 + P^2, \tag{7}$$

where Z is intuitively proportional to the intensity or the photon number of the input states.

Given the input signal states of interferenced beam is a photon number state (Fock state $|n\rangle$), in the case of every one-shot measurement, the probability density function of a measured photon number z from the input interferenced beam satisfies [21]:

$$P_Z(Z = z|n) = e^{-z}\frac{z^n}{n!}, \tag{8}$$

where n is the average input photon number.

Whether the detection outcome "a vacuum state" or "a state with left photons", referred as "the $\hat{D}(\beta_i)$ is prepared as the same as the $|\alpha_k\rangle$" or not, is generally obtained from single photon detectors in the conventional quantum receiver. Such the detection outcome could also be recovered by the conjugated homodyne detectors and be recorded by the FPGA in our proposed CHD quantum receiver. The corresponding records will be processed as a feedback to order the next preparation step towards the displacement operator $\hat{D}(\beta_i)$, as Fig. 2 shown. The detailed description on feedback circuit could be referred in Appendix A.

Similarily, to discriminate detection of the vacuum state or non-vacuum state, the continuous single-shot measurement result (detected photon statistic under realistic detector) z is required to be mapped with the possible detection outcome of "click or no click" of the conjugated homodyne detector. Here, a pre-design detection threshold $\tau \in [0, +\infty)$ of the conjugated homodyne detector is set to distinguish the detection outcome as well as the relative detection events [21, 22]. The output of the detector will be regarded as click/no click when the measurement result z is larger/smaller than the threshold τ. Such mapping process could be applied in the post-processing stage under a proper threshold τ to obtain the lowest error probability on QPSK states discrimination.

Then we evaluate the performance of the conjugated homodyne detector under photon counting mode as a threshold SPD which can only distinguish vacuum states from non vacuum states rather than resolve photon number. And the detection efficiency η and dark count rate ν, two important factors defined as the conditional probability that the SPD clicks whether the input states obtain photons or not, will satisfy the following equation in the conjugated homodyne detectors by Eq. (8):

$$\eta = \int_{\tau}^{\infty} P_Z(Z = z|1)\, dz = e^{-\tau}(\tau + 1), \tag{9}$$

$$\nu = \int_{\tau}^{\infty} P_Z(Z = z|0)\, dz = e^{-\tau}. \tag{10}$$

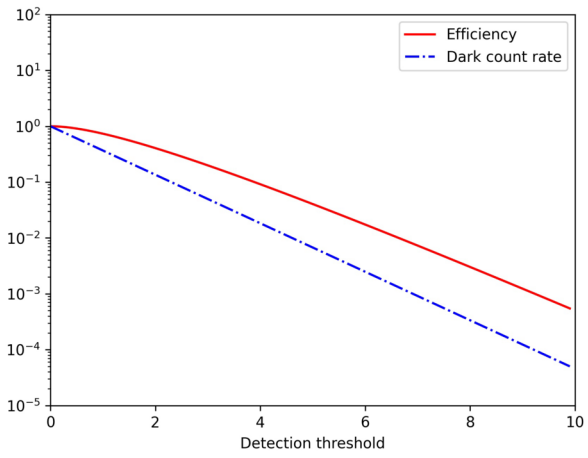

Figure 3 Detection efficiency η and dark count rate ν against detection threshold τ

As both detection efficiency η (red line) and dark count rate ν (blue dash-dot line) are present as functions of the threshold τ in Fig. 3, it is clear that both the detection efficiency and the dark count rate will drop as the value of the detection threshold rises. We cannot have a high detection efficiency and low dark count at the same time. Therefore, a proper threshold are deserved to be explored for a better detection performance (higher efficiency as well as a lower dark count rate) of the conjugated homodyne detection.

Moreover, given that our conjugated homodyne detector consisting of 4 detectors with unity efficiency η_{det} and an enough strong LO, the conjugated homodyne detector can be regarded equally as a virtual beam splitter (transmission efficiency η_{det}) together with 4 ideal detectors (detection efficiency 100%). The equivalent model of the conjugated homodyne detector towards detection efficiency will be discussed in Appendix B. As 4 detectors with realistic unity efficiency η_{det} taken into account, the detection efficiency η_{CHD} of the conjugated homodyne detector can be concluded based on Eq. (9):

$$\eta_{\text{CHD}} = \eta_{\text{det}}\eta = \eta_{\text{det}}e^{-\tau}(\tau + 1). \tag{11}$$

Thus, the initial error probability of detection $P(e_i = 0|\alpha_k; \beta_i)$ from the conventional quantum-enhanced receiver in Eq. (2) will be modified by the detection parameters—the detection efficiency η_{CHD} and dark count rate ν from the Eq. (11) and Eq. (10) under "photon counting"mode in conjugated homodyne detection:

$$P(e_i = 0|\alpha_k; \beta_i) = e^{-e^{-\tau}[1+\eta_{\text{det}}(\tau+1)|\alpha_k-\beta_i|^2]}, \tag{12}$$

where τ denotes the pre-designed detection threshold in the conjugated homodyne detectors. Moreover, as the displacement operator $\hat{D}(\beta_i)$ is modulated to have the same amplitude as the amplitude of the signal state $|\alpha_k\rangle$. We could take the photon number $|\alpha_k - \beta_i|^2$ of the interference light in Eq. (3) into consideration and the final formula of the detection probability will be obtained:

$$P(e_i = 0|\alpha_k; \beta_i) = e^{-e^{-\tau}[1+2\eta_{\text{det}}(\tau+1)(1-\xi\cos\theta)|\gamma|^2]}. \tag{13}$$

Based on Eq. (4), the average error probability for distinguishing the QPSK coherent states in our CHD quantum-enhanced receiver could be obtained as:

$$P_e = 1 - \frac{1}{4}\sum_{m=0}^{3}\sum_{\{\beta_i,e_i\}\in\Theta_k} P\big(\{\beta_i, e_i = 0\}|\alpha_k\big). \tag{14}$$

4 Results and discussion

Based on the simulation model with Eqs. (13) and (14), we evaluated the average error probability for QPSK state discrimination through Monte Carlo simulations. We change the detection threshold τ of the conjugated homodyne detectors to explore a proper value to pursue a lower error probability of our CHD quantum-enhanced receiver. And we compare the simulation outcome with the detection performance of the conventional quantum-enhanced receiver with SNSPDs under different detection efficiency, trying to figure out to what extend our CHD quantum-enhanced receiver can match the performance on discriminating coherent states. All the simulations are conducted under the same parameters from reported experiments.

4.1 The average error probability of CHD quantum-enhanced receiver against different τ

The theoretical value of the two imperial parameters: dark count rate (for per state) $\nu = 9.1 \times 10^{-3}$ and interference visibility $\xi = 99.6\%$ in our simulation are taken from the reported references [12, 14] under experimental conditions. And 4 commercial detectors with unity typical efficiency $\eta_{\text{det}} = 0.85$ are taken into account.

Based on the designed parameters, we conduct the simulation on discriminating every 10^5 QPSK coherent states under the time-bin parts $M = 4, 8$ and 12, respectively. The outcome are depicted as Fig. 4 shown.

Among Fig. 4, a dashed line and a thick dash-dotted line represent the Helstrom bound and the SQL, respectively. And it is clear that a better performance (lower error probability) of our CHD quantum-enhanced receiver can be obtained as more time-bin parts M are taken to be tested by more displacement operators.

For $M = 4$, no matter what value of the detection threshold τ is taken, the SQL seems to be a barrier for our CHD quantum-enhanced receiver to cross over. The reason can be concluded as follows: every input signal state $|\alpha_k\rangle$ is divided into only 4 parts, making the preparation of displacement operator $\hat{D}(\beta_i)$ just going through 4 different states in the QPSK protocol. During the period of each state $|\alpha_k\rangle$, the detection on every interference between the $|\alpha_k\rangle$ and different $\hat{D}(\beta_i)$ can be regarded as an isolated classical homodyne detection, bring no effective adaptive feedback to enhance the correct rate of discrimination. As more parts are divided in each input state $|\alpha_k\rangle$, more chances will be left to prepare different $\hat{D}(\beta_i)$ based on the former detection outcome. More trials are made, the higher probability will be obtained to get $\hat{D}(\beta_i)$ the same as $|\alpha_k\rangle$. Therefore, when $M = 8$, the error probability of the CHD quantum-enhanced receiver is getting lower as the detection threshold τ is smaller. Especially, when τ is smaller than 0.7, the SQL is beat with the input average photon number from 2 to 8. The detection performance takes a huge leap for $M = 12$ on the whole. The error probability for CHD quantum-enhanced receiver gets lower as the decrease of detection threshold τ from 2 to 0.3. This can be concluded from Fig. 3 that the decrease of τ leads to the elevation of both efficiency η and dark count

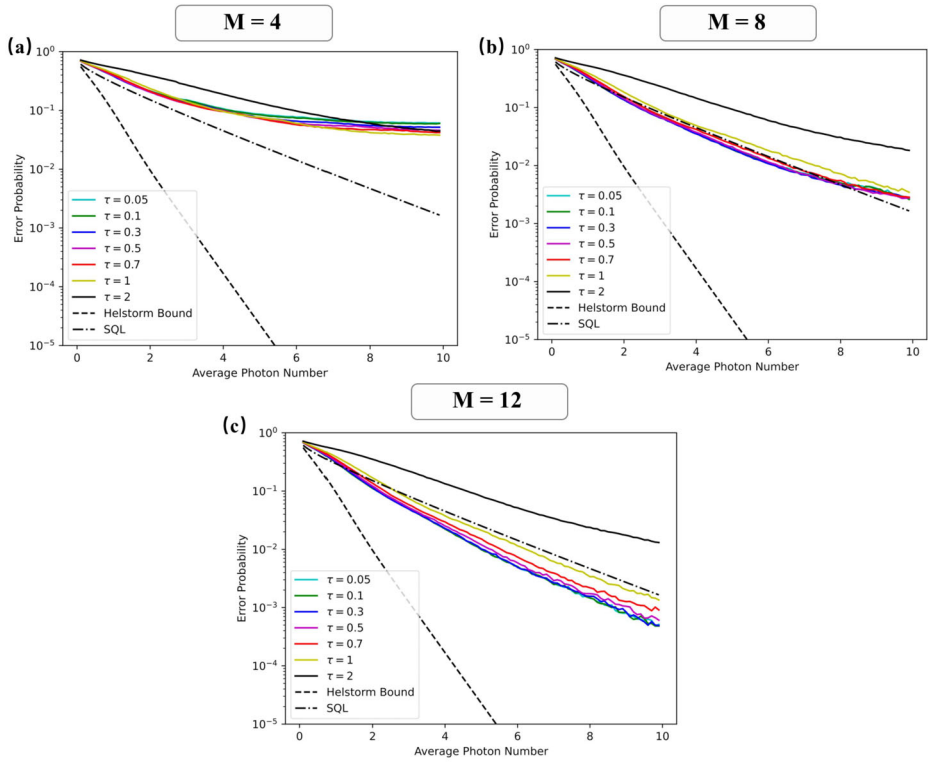

Figure 4 For different separations (**a**) $M = 4$, (**b**) $M = 8$ (**c**) $M = 12$, the average error probability of CHD quantum-enhanced receiver with different pre-design detection threshold τ against average photon number

rate ν while the detection efficiency η plays a more important role on the detection performance of CHD quantum-enhanced receiver. When $\tau = 0.05$, 0.1 and 0.3, there is no clear difference that the CHD quantum-enhanced receiver get the lowest error probability for both $M = 8$ and $M = 12$. Therefore, as we set detection threshold τ from 0.05 to 0.3, we can not only obtain the lowest error probability on state discrimination, but also strike a balance between a higher detection efficiency and lower dark count in Fig. 3.

4.2 The performance comparison between the CHD quantum-enhanced receiver and the conventional quantum-enhanced receiver with SNSPDs under different detection efficiencies

As the proper detection threshold τ from 0.05 to 0.3 is selected, our CHD quantum-enhanced receiver has achieved its theoretical lowest average error probability, which largely beat the SQL while is still far behind the Helstrom bound. In this section, we try to explore to what extend our CHD quantum-enhanced receiver can match the performance of the conventional quantum-enhanced receiver with SNSPD under different detection efficiencies.

Similarily, both the CHD quantum-enhanced receiver and the conventional quantum-enhanced receiver have a better performance as the number of the separations M is larger as Fig. 5 shown. For $M = 4$, the conventional quantum-enhanced receiver with SNSPDs under different efficiency 50%–90% all surpass the performance of the CHD quantum-enhanced receiver with the average photon number of input states more than 4. When $M = 8$, the error probability of the CHD quantum-enhanced receiver with $\tau = 0.5, 0.1$ and 0.3

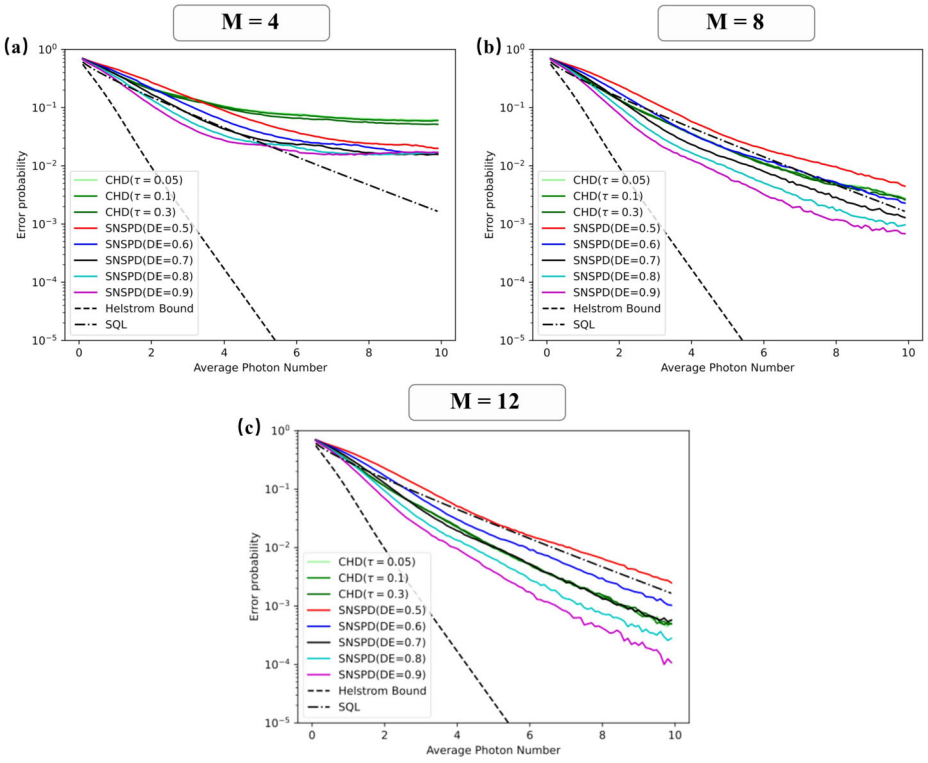

Figure 5 For time-bin separations (**a**) $M = 4$, (**b**) $M = 8$ and (**c**) $M = 12$, the average error probability of the CHD quantum-enhanced receiver ($\tau = 0.05, 0.1$ and 0.3) and conventional quantum-enhanced receivers with SNSPDs under different detection efficiency against average photon number

(for light green, green and dark green lines respectively) all beats the SQL, being in line with the conventional quantum-enhanced receiver with the SNSPD's efficiency of 60% (dark blue line) as the average photon number is under 8. However, the performance of the CHD quantum-enhanced receiver degrades when the average photon number is over 8. It can be explained that CHD quantum-enhanced receivers has difficulties on distinguishing coherent states when a large number of photons crowd in. And for $M = 12$, our CHD quantum-enhanced receiver has caught up with the conventional quantum-enhanced receiver performance under its SNSPD's efficiency of 70% (black line), beating the SQL with a huge advantage.

Based on the selected detection threshold τ from 0.05 to 0.3, the performance of our CHD quantum-enhanced receiver is comparable to the conventional quantum-enhanced receivers with its SNSPD's efficiency of 60% for $M = 8$ and 70% for $M = 12$, respectively. The simulation outcome has implied that conjugated homodyne detectors are suitable for application in the quantum-enhanced receiver and the proposed CHD quantum-enhanced receiver has a great potential to take the place of the high-detection-efficiency conventional quantum-enhanced receiver on discriminating QPSK coherent states.

5 Conclusions

Based on the reported theoretical analysis that the received photon number of a quantum state can be reconstructed, the conjugated homodyne detector can work as an SPD on distinguishing whether a photon is received or not. We firstly proposed a novel structure of

CHD quantum-enhanced receiver consisting of a displacement operation, two commercial conjugated homodyne detectors, and feedback operation. Through our simulations, as the proper detection threshold τ from 0.05 to 0.3 is selected, the conjugated homodyne detectors strike a balance between low dark count rate and high detection efficiency. And the CHD quantum-enhanced receiver obtains the ability of discriminating QPSK signals with an error probability beating the SQL at telecom wavelength. We further investigate the performance between our CHD quantum-enhanced receiver with conjugated homodyne detectors and the conventional quantum receiver with commercial SNSPDs. It is worth noting that our CHD quantum-enhanced receiver is comparable with the performance of the conventional quantum-enhanced receiver with its commercial SNSPD's efficiency from 60% to 70%, which means conjugated homodyne detectors can be a more cheap alternative for SNSPDs in conventional quantum-enhanced receiver to some extent.

Our work has explored the potential of applying the conjugated homodyne detectors to the quantum-enhanced receiver. As far as we can see, this is the first time to propose the novel CHD quantum-enhanced receiver with a comparable performance on distinguishing QPSK states. Due to the lower cost and room-temperature operation of the CHDs, our proposed quantum-enhanced receiver is expected to be more suitable for applications like continuous-variable quantum key distribution, long-distance coherent optical communication especially for commercial scenes which requests room-temperature working condition and massive production. Additionally, capable of discriminating coherent laser signals with average low intensity (only several photon numbers), the CHD quantum-enhanced receiver could also be practically applied to deep space communication links to enhance the power budget of satellites or increase the free-space communication range and communication rates. Meanwhile, the elevation on the performance of our proposed CHD quantum-enhanced receiver could also be witnessed soon as higher-quality conjugated homodyne detectors are applied or a more exquisite detection structure is designed.

Appendix A: Analysis of feedback circuit

Based on the analysis of the quantum-enhanced receiver shown in Fig. 1 and Fig. 2, the theoretical model of feedback circuit is illustrated as Fig. A.

Firstly, coherent states $|\alpha_k\rangle = ||\alpha|e^{\frac{(2k+1)i\pi}{4}}\rangle$, $k = 0, 1, 2, 3$ with one spatial mode is prepared in a square pulse with a time width of T. Each pulse will be encoded randomly from QPSK protocol (here, we take a pulse with its encoded state $|\alpha_1\rangle$ as an example shown in Fig. A). Then we virtually separated the pulse to M parts and prepare different kind of displacement operator $\hat{D}(\beta_i)$, $i = 0, 1, 2, 3$ from QPSK protocol during parts from 1 to M one by one.

During 1st part, assuming that we prepare a displacement $\hat{D}(\beta_2)$ to interference with input coherent state $|\alpha_1\rangle$ in the beam splitter (or an optical coupler in Fig. 2). A priori belief was that the displacement operators is encoded as same as the input coherent state, and the input coherent state $|\alpha_1\rangle$ will be shifted to vacuum state with no photons detected (detection event satisfies $e_i = 0$), this belief would be ensured and the same displacement operator $\hat{D}(\beta_2)$ would be maintained for the next preparation. If not, photons will be left in the output interferenced beam and be detected by the conjugated homodyne detector

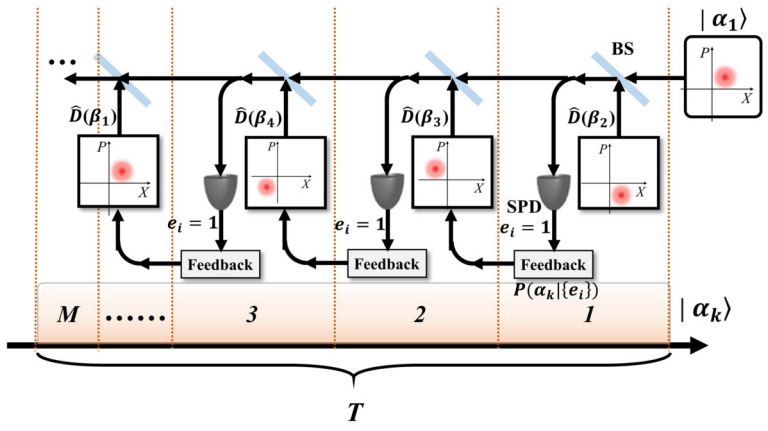

Figure A The schematic of the feedback circuit in our proposed CHD quantum-enhanced receiver, BS, beam splitter; SPD, single photon detector

(detection event satisfies $e_i = 1$). And another displacement operator ($\hat{D}(\beta_3)$ for example) would be prepared for the 2nd part. The detection event history $\{e_i\}$ will be recorded by and the instruction of preparing next displacement operator (maintained or changed) will be transformed from digital to analogue by DAC module. Similar process will be repeated in the following parts along the whole pulse duration T.

For the jth part, on the basis of the photon-detection history $\{e_i\}$, input state $|\alpha_k\rangle$ and the current preparation displacement operator $\hat{D}(\beta_i)$, the posteriori probability after detection could be obtained by:

$$P\big(\alpha_k|\{\beta_i, e_i = 0\}\big) = \frac{\Pi_{h=1}^{j} P(e_h|\alpha_k/\sqrt{M};\beta_h)}{\sum_{l=0}^{3}\Pi_{h=1}^{j} P(e_h|\alpha_l/\sqrt{M};\beta_h)}. \tag{A}$$

Appendix B: Models of realistic detectors with detection efficiency

According to [28], given the LO is enough strong, a single DC-balanced homodyne detector consisting two detectors with efficiency η_D can be modeled by the one that a virtual beam splitter with transmission efficiency η_D before the input port of ideal detectors (efficiency 100%). Therefore, 4 lossy detectors with unity efficiency η_{det} in the conjugated homodyne detector can be replaced as 4 beam splitter with transmission efficiency η_{det} before 4 ideal detectors (efficiency 100%) respectively, as shown in Fig. B(a).

Furthermore, when a conjugated homodyne detector is applied to recover the photon statistics of input signal under photon-counting mode, Ref. [21] has verified that the a conjugated homodyne detector consisting of 4 lossy detectors (with unity efficiency η_{det}) are equivalent as the one consisting 4 ideal detectors while a beam splitter with transmission efficiency η_{det} virtually placed before the input port of signal. Two models in Fig. B are equivalent to each other.

Hence, to calculate the equivalent detection efficiency of the conjugated homodyne detector, the additional unity efficiency η_{det} of 4 lossy detectors have been taken into account, as Eq. (11) shown.

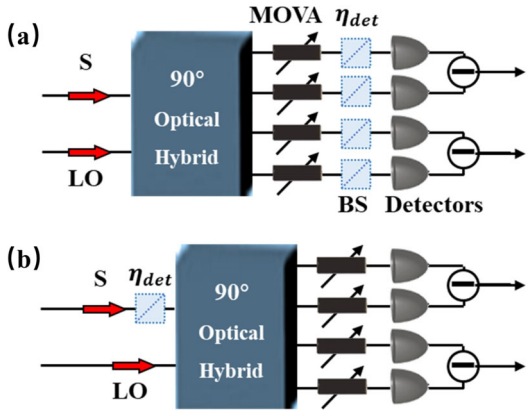

Figure B Models of proposed conjugated homodyne detector (4 noiseless detectors with unity efficiency η_{det}). (**a**) The actual setup (**b**) An equivalent model of actual setup

Acknowledgements
Not applicable.

Funding
This work is supported by the National Key Basic Research Program of China (2021-JCJQ-JJ-0510), the Scientific Research Program of National University of Defense Technology, China (ZK22-09), the Independent Innovation Science Fund Program of National University of Defense Technology, China (22-ZZCX-036).

Abbreviations
QPSK, quadrature phase shift keying; CHD, conjugated homodyne detection; QKD, quantum key distribution; SQL, standard quantum limit; HB, helstrom bound; SPD, single photon detector; SNSPD, superconducting nanowire single photon detector; PNRD, photon number resolving detector; TES, transition edge sensor; POVM, positive operator valued measure; CW, continuous wave; LO, local oscillator.

Availability of data and materials
Simulated data and calculations during the current study are available from the corresponding author upon a reasonable request.

Declarations

Ethics approval and consent to participate
Not applicable.

Consent for publication
Not applicable.

Competing interests
The authors declare no competing interests.

Author contributions
The model design and simulations were done by WTY and DC. The background was analyzed by RY and ZZC. GC and LK handled the verification of manuscript. The effort was conceived and supervised by RY and DC. WTY wrote the draft and all authors reviewed the manuscript. All authors read and approved the final manuscript.

Received: 4 December 2022 Accepted: 18 April 2023 Published online: 02 May 2023

References
1. Helstrom C. Mathematics in science and engineering. New York: Academic Press; 1976. p. 123.
2. Kok P, Munro WJ, Nemoto K, Ralph TC, Dowling JP, Milburn GJ. Rev Mod Phys. 2007;79.
3. Knill E, Laflamme R, Milburn GJ. Nature. 2001;409(6816):46–52.
4. Xiao T, Fan J, Zeng G. npj Quantum Inf. 2022;8(1):2.
5. Giovannetti V, Lloyd S, Maccone L. Nat Photonics. 2011;5(4):222–9.
6. Giovannetti V, Lloyd S, Maccone L. Phys Rev Lett. 2006;96(1):010401.
7. Van Enk SJ. Phys Rev A. 2002;66(4):042313.
8. Banaszek K. Phys Lett A. 1999;253(1):12–5.
9. Bennett CH. Phys Rev Lett. 1992;68(21):3121–4.
10. Tsujino K, Fukuda D, Fujii G, Inoue S, Fujiwara M, Takeoka M, Sasaki M. Phys Rev Lett. 2011;106(25):250503.

11. Sidhu JS, Izumi S, Neergaard-Nielsen JS, Lupo C, Andersen UL. PRX Quantum. 2021;2(1).
12. Izumi S, Neergaard-Nielsen JS, Andersen UL. PRX Quantum. 2021;2(2).
13. Shcherbatenko ML, Elezov MS, Goltsman GN. Phys Rev A. 2020;101(3):032306.
14. Izumi S, Neergaard-Nielsen JS, Miki S, Terai H, Andersen UL. Phys Rev Appl. 2020;13(5):054015.
15. Mikhail Elezov MS, Denis S, Gregory G. EPJ web of conferences IWQO-2019. 2019.
16. Burenkov IA, Jabir MV, Polyakov SV. AVS Quantum Sci. 2022;3:025301.
17. Habif JL, Jagannathan A, Gartenstein S, Amory P, Guha S. Opt Express. 2021;29(5):7418–27.
18. Izumi S, Takeoka M, Wakui K, Fujiwara M, Ema K, Sasaki M. Phys Rev A. 2016;94(3):033842.
19. Becerra FE, Fan J, Migdall A. Nat Photonics. 2015;9(1):48–53.
20. Izumi S, Takeoka M, Ema K, Sasaki M. Phys Rev A. 2013;87(4):042328.
21. Qi B, Lougovski P, Williams BP. Opt Express. 2020;28(2):2276–90.
22. Qi B. Phys Rev A. 2021;103(1):012606.
23. Ramos FM, Pinto NA, Silva AN. Sci Rep. 2022;12:6135.
24. Primaatmaja IW, Liang CC, Zhang G, Haw JY, Wang C, Lim CC-W. Quantum. 2022;6(613).
25. Barnett SM, Phillips LS, Pegg DT. Opt Commun. 1998;158(1):45–9.
26. Becerra FE, Fan J, Baumgartner G, Goldhar J, Kosloski JT, Migdall A. Nat Photonics. 2013;7(2):147–52.
27. Becerra FE, Fan J, Baumgartner G, Polyakov SV, Goldhar J, Kosloski JT, Migdall A. Phys Rev A. 2011;84(4):062324.
28. Leonhardt U, Paul H. Phys Rev A. 1993;48(6):4598.

Publisher's Note